A Model for the Free Radical and Electrophilic Hydroxylation of Bicyclo[2.1.0]pentane

Robert D. Bach,*,† H. Bernhard Schlegel,† José L. Andrés,‡ and Carlos Sosa§

Contribution from the Department of Chemistry, Wayne State University, Detroit, Michigan 48202, Department of Chemistry, University Autonoma of Barcelona, 08193 Bellaterra, Catalonia, Spain, and Cray Research, Inc., 655 East Lone Oak Drive, Eagan, Minnesota 55120

Received June 16, 1993. Revised Manuscript Received January 21, 1994®

Abstract: Ab initio molecular orbital calculations have been used to model the stereochemistry of bicyclo[2.1.0]pentane hydroxylation. Equilibrium geometries and transition states were fully optimized at the MP2 level of theory using the 6-31G* and 6-31G** basis sets; all transition states were confirmed to be first-order saddle points by MP2 frequency calculations; energy differences and barrier heights were computed at the MP4 level with and without spin projection. Both the *endo*- and *exo*-bicyclo[2.1.0]pent-2-yl radicals are significantly pyramidal, but are nearly equal in energy (ΔE < 0.3 kcal/mol) and are separated by a very low (<0.4 kcal/mol) barrier. The barrier for trapping the bicyclopentyl radical by H_2S is 1.5 kcal/mol lower for the *endo* radical. Even though the *endo* and *exo* bond strengths are nearly identical in bicyclo[2.1.0]pentane, abstraction of the *endo* hydrogen via the OH radical is favored over the *exo* hydrogen by 1.4 kcal/mol. Concerted oxygen insertion was modeled by reaction of bicyclo[2.1.0]pentane with water oxide, H_2OO; the insertion transition state yielding the *endo* alcohol is 1.3 kcal/mol lower in energy. The *endo* preference of all the reactions in the present study can be attributed to cyclopropylcarbinyl stabilization of the transition states. The relevance of these calculations to cytochrome P-450 hydroxylation is discussed.

Introduction

One of the most intriguing oxidations mediated by cytochrome P-450 (P-450) involves the hydroxylation of unactivated carbon–hydrogen bonds.[1] Early mechanistic studies suggested that oxygen atom transfer to the alkane substrate occurred by a concerted oxene insertion process. In many cases hydroxylation occurred with essentially complete stereoselectivity.[2] With the increased capability to measure very fast reaction rate constants (10^9–10^{12} s^{-1}) approaching molecular vibration time scales, the realization that a multistep oxygen-transfer process could also proceed with retention of configuration is gaining acceptance. The currently accepted mechanism for alkane hydroxylation involves two discrete reactions: first, abstraction of a hydrogen atom from the substrate by an oxoiron species (Fe^{IV}=O) (eq 1), and secondly, a rapid collapse of the resulting carbon radical–hydroxyferryl complex to give the product alcohol and the resting-state enzyme (eq 2).

(Eq. 1)

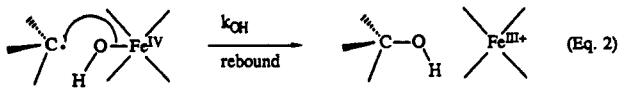

(Eq. 2)

This oxygen-rebound mechanism proposed by Groves et al. has also been extended to hydroxylation reactions mediated by nonenzymatic iron porphyrin catalysts.[3] Bicyclo[2.1.0]pentane (**1**) has been used as a calibrated free-radical "clock"[4] with which the rate of oxygen rebound (k_{OH}) may be determined by measuring the ratio of insertion product **4** that is derived from bicyclo-[2.1.0]pent-2-yl radical (**2**) to the amount of rearranged alcohol **5** resulting from capture of hydroxyl radical by cyclopent-3-enyl radical (**3**) (Scheme 1). Ortiz de Montellano and Stearns[5] examined the P-450 hydroxylation of **1** and established a 7:1 ratio of unrearranged (**4**) to rearranged (**5**) alcohols, suggesting that the oxygen rebound (k_{OH}) is about seven times faster than the ring opening (k_r) of the bicyclo[2.1.0]pent-2-yl radical.[6a] Selective abstraction of the *endo*-C-2 hydrogen and formation of only the *endo*-C-2 alcohol **4** were ascribed to geometric constraints imposed by the enzyme active site. Newcomb et al.[7a] have measured the relative rate constants (k_r/k_H) for ring opening of bicyclo[2.1.0]pent-2-yl and trapping of radical **2** with RSH and have reported a value of k_r at 25 °C of 1.5×10^9 s^{-1}. Highly stereoselective trapping of **2** with ArSD afforded *exo*- to *endo*-bicyclo[2.1.0]pentane-d_2 in a ratio of 6:94. The small kinetic isotope effect (k_H/k_D = 1.85) observed is consistent with a slight S–D bond breaking in the transition state for the exothermic deuterium atom transfer reaction. It was suggested that the high stereoselectivity was a consequence of a stereoelectronic effect between the C-1–C-4 bond and the *endo*-C-2–H bond. Wiberg et al.[8] have predicted on the basis of ab initio calculations at the HF/6-31G* level that the *endo*-C-2–H bond is 0.0022 Å longer than the *exo*-C-2–H bond. Since *endo* trapping was favored by a $\Delta\Delta G^{\ddagger}$ of about 1.1 kcal/mol, microscopic reversibility arguments

† Wayne State University.
‡ University Autonoma of Barcelona.
§ Cray Research, Inc.
• Abstract published in *Advance ACS Abstracts,* March 15, 1994.

(1) (a) *Cytochrome P-450: Structure Mechanism and Biochemistry*; Ortiz de Montellano, P. R., Ed.; Plenum: New York, 1986. (b) Ortiz de Montellano, P. R. *Acc. Chem. Res.* **1987**, *20*, 289.
(2) Hayano, M. In *Oxygenases*; Hayaishi, O., Ed.; Academic Press: New York, 1986; pp 181–240.
(3) Groves, J. T.; McClusky, G. A.; White, R. E.; Coon, M. *J. Biochem. Biophys. Res. Commun.* **1978**, *81*, 154.
(4) Griller, D.; Ingold, K. U. *Acc. Chem. Res.* **1980**, *13*, 317.
(5) Ortiz de Montellano, P. R.; Stearns, R. A. *J. Am. Chem. Soc.* **1987**, *109*, 3415.
(6) (a) Anell, P. L.; Biffi, C.; Montanari, F.; Quill, S. *J. Org. Chem.* **1987**, *52*, 2559. (b) Bowry, V. E.; Lusztyk, J.; Ingold, K. U. *J. Am. Chem. Soc.* **1989**, *111*, 1927. (c) Bowry, V. W.; Ingold, K. U. *J. Am. Chem. Soc.* **1991**, *113*, 5699. (d) Bowry, V. W.; Lusztyk, J.; Ingold, K. U. *J. Am. Chem. Soc.* **1991**, *113*, 5687. (e) Bowry, V. W.; Lusztyk, J.; Ingold, K. U. *Pure Appl. Chem.* **1990**, *62*, 213.
(7) (a) Newcomb, M.; Manek, M. B.; Glenn, A. G. *J. Am. Chem. Soc.* **1991**, *113*, 949. (b) Newcomb, M.; Johnson, C. C.; Manek, M. B.; Varick, T. R. *J. Am. Chem. Soc.* **1992**, *114*, 10915. (c) Newcomb, M. *Tetrahedron* **1993**, *49*, 1151.
(8) Wiberg, K. B.; Bader, R. F. W.; Lau, C. D. H. *J. Am. Chem. Soc.* **1987**, *109*, 985, 1001.

0002-7863/94/1516-3475$04.50/0

Scheme 1

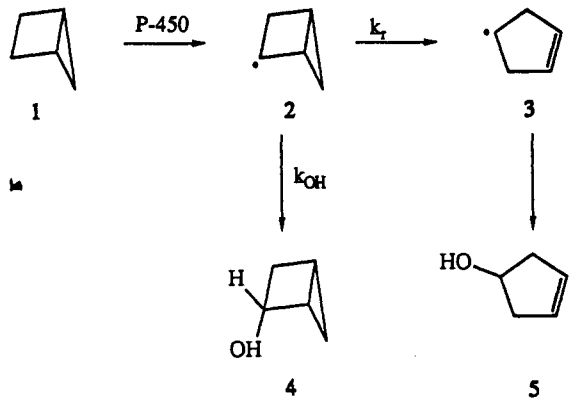

suggest that the *endo*-C-2 hydrogen in **1** must also be abstracted by PhS• more readily than the *exo*-C-2 hydrogen, possibly reflecting the difference in bond strengths of the *exo* and *endo* hydrogens. The origins of this selectivity, however, are quite complex since the radical–radical coupling of radical **2** with the nitroxyl radical Tempo[6a] gave the *exo* adduct as the major product with an *exo*:*endo* ratio of 2.4:1.[6b-e]

In this report we will examine the electronic structure of bicyclo[2.1.0]pentane (**1**), its free radical, **2**, and the relative reactivity of the *exo* and *endo* hydrogens of **1** toward abstraction, free-radical trapping, and electrophilic oxygen insertion.

Method of Calculation

Molecular orbital calculations were carried out using the Gaussian 92 program system[9a] utilizing gradient geometry optimization.[9b] Unrestricted Hartree–Fock and Møller–Plesset perturbation theories[9c] were used for all open-shell species; restricted methods were used for closed-shell systems. Preliminary geometries of the reactants and transition structures were first determined at the second-order Møller–Plessett (MP2) level of theory with the 3-21G basis set. All geometries were then fully optimized with the 6-31G* or 6-31G** basis set using second-order pertubation theory unless noted otherwise. Relevant energies and barrier heights for oxygen insertion into **1** by water oxide were computed using fourth-order Møller–Plesset perturbation theory and the MP2-optimized geometry (frozen core, MP4SDTQ/6-31G*//MP2/6-31G* or MP4/6-31G**//MP2/6-31G**). Vibrational frequency calculations at the MP2 level[9d] were used to characterize these stationary points as either minima (zero imaginary frequencies), first-order transition states (a single imaginary frequency), or second-order saddle points, SOSP (two imaginary frequencies).

The potential energy surfaces for radical trapping of **2** with H_2S were examined at the MP2/6-31G** (frozen core) level. Vibrational frequency calculations at the MP2/6-31G** level established both *endo* and *exo* transition states as first-order saddle points. The transition structures for *endo* and *exo* hydrogen abstraction from **1** with HO• were also calculated at the MP2/6-31G** (full) level, and an analytical frequency calculation at the same level of theory established both transition states to be first-order saddle points. Entropies were calculated in the rigid rotor–harmonic oscillator approximation (no special treatment for low-frequency modes).

Results and Discussion

Bicyclo[2.1.0]pent-2-yl Radical. Since the bicyclo[2.1.0]pent-2-yl radical (**2**) is the putative intermediate in P-450 hydroxylation of this hydrocarbon,[5] we initiated this study with an examination of its geometry. MINDO/3 calculations have suggested that free radical **2** has a nonplanar radical center that is only 0.05 kcal/mol lower in energy than the radical when it was forced to be planar.[10] The present ab initio calculations[9a] with full geometry optimization at the MP2/6-31G* level also predict that the radical is nonplanar. There are two minima on the MP2/6-31G* hypersurface, with *exo* radical **2** predicted to be 0.19 kcal/mol more stable than *endo* radical **2** (Table 1). The deviation of the radical center from planarity, as measured by the C_1–C_2–C_3–H_1 dihedral angle β (Figure 1), is –23.4° for the *exo* radical **2**, while β is 36.4° for the *endo* radical. This is perhaps not too surprising because nonplanar cyclopropylcarbinyl cations have been invoked in the explanation of highly stereoselective solvolysis reactions.[11] Stereoelectronic effects due to cyclopropylcarbinyl stabilization also dramatically influence the rate of solvolysis of *exo*- and *endo*-bicyclo[2.1.0]pentyl 3,5-dinitro-2-benzoate, where a difference in activation enthalpy of 12 kcal/mol and an *endo*:*exo* rate ratio of 10^7 have been reported.[12] The observed ratio of alcohols (**4**:**5**) derived from P-450 oxidation can also be influenced by rearrangement of **4** under the polar conditions of the experiment.[6b]

The transition state (TS-**6**) connecting the two nonplanar radicals has a very small activation barrier (0.39 kcal/mol) at the MP2/6-31G* level, and this activation barrier was found to be identical with the 6-31G** basis set. Although TS-**6** was established to be a first-order saddle point by an analytical frequency calculation at the MP2/6-31G* level, the small barrier disappears when corrections for zero-point energy (ZPE) are added. Fourth-order Møller–Plesset treatment of electron correlation has essentially no effect upon the magnitude of these relatively small energy differences (Figure 1). With spin projection[9c] (PMP4//MP2/6-31G*) TS-**6** and *endo*-**2** have virtually identical energies, and both are 0.25 kcal/mol above the global minimum, *exo*-**2**. This overall potential energy surface is extremely shallow, and relative energies of this magnitude should not exert a discernible influence upon the stereoselectivity of radical trapping. Since the *endo* and *exo* free radicals are of the same energy, the *exo*- and *endo*-C-2–H bonds must also have the same bond strength.

Radical Trapping with Dihydrogen Sulfide. Radical recombination reactions of bicyclo[2.1.0]pent-2-yl radical (**2**) with nitroxyl radical[6] occurred predominantly from the *exo* face of **2**, suggesting that C–O bond formation was controlled by steric factors. However, carbon–hydrogen bond formation in trapping experiments of radical **2** with ArSH proceeded almost exclusively (96:4) from the more hindered *endo* face. The stereoselectivity was reduced with the more reactive trapping agent ArSeH. An earlier transition state was implicated in the explanation of the reactivity differences.[7a]

In an effort to examine the stereoelectronic influence of the cyclopropylcarbinyl radical on the *endo*:*exo* ratio of radical trapping, we have examined potential energy surfaces for the reaction of radical **2** with H_2S at the MP2/6-31G** level of theory. At the MP4/6-31G**//MP2/6-31G* level of theory the *endo* transition state (TS-**7**) has a predicted $\Delta E^{\ddagger} = 1.0$ kcal/mol (Figure 2). The barrier height for hydrogen transfer from H_2S to the *endo* face of **2** was 1.5 kcal/mol lower than radical trapping from the *exo* direction, in excellent agreement with experiment. With ZPE corrections the MP2/6-31G** barriers for TS-**7** and TS-**8** change by 0.03 and 0.17 kcal/mol. The PMP4/6-31G**//MP2/6-31G** barrier heights for TS-**7** and TS-**8** are 0.44 and 1.79 kcal/mol, respectively. Note that the relative barrier heights for *exo* versus *endo* change by less than 0.3 kcal/mol on going from the MP2 to the PMP4 level of theory. Both transition structures were established to be first-order saddle points at both

(9) (a) Frisch, M. J.; Trucks, G. W.; Head-Gordon, M.; Gill, P. M. W.; Wong, M. W.; Foresman, J. B.; Johnson, B. G.; Schlegel, H. B.; Robb, M. A.; Replogle, E. S.; Gomperts, R.; Andrés, J. L.; Raghavachari, K.; Binkley, J. S.; Gonzalez, C.; Martin, R. L.; Fox, D. J.; Defrees, D. J.; Baker, J.; Stewart, J. J. P.; Pople, J. A. *GAUSSIAN 92*; Gaussian, Inc.: Pittsburgh, PA, 1992. (b) Schlegel, H. B. *J. Comput. Chem.* **1982**, *3*, 214. (c) Møller, C.; Plesset, M. S. *Phys. Rev.* **1934**, *46*, 618. (d) Trucks, G. W.; Frisch, M. J.; Head-Gordon, M.; Andrés, J. L.; Schlegel, H. B.; Salter, E. A. *J. Chem. Phys.*, submitted for publication. (e) Schlegel, H. B. *J. Chem. Phys.* **1986**, *84*, 4530; **1988**, *92*, 3075.

(10) Bews, J. R.; Glidewell, C.; Walton, J. C. *J. Chem. Soc., Perkin Trans. 2*, **1982**, 1447.

(11) Bach, R. D.; Blanchette, P. E. *J. Am. Chem. Soc.* **1979**, *101*, 46.

(12) Wiberg, K. B.; Williams, V. Z., Jr.; Friedrich, L. E. *J. Am. Chem. Soc.* **1970**, *92*, 564.

Table 1. Total Energies in Hartrees[a]

compound	MP2/6-31G*	MP4/6-31G*// MP2/6-31G*	MP2/6-31G**	MP4/6-31G**// MP2/6-31G**	PMP4//MP2[b]	ZPE corr[b]
1	−194.598 97	−194.644 79	−194.664 96	−194.712 59		0.119 79[c]
exo-**2**	−193.941 40	−193.986 63	−193.973 52	−194.045 94	−193.988 17[c]	0.104 85[c]
					−194.047 48[d]	0.105 25[d]
endo-**2**	−193.941 10	−193.986 30			−193.987 77	
4 (*endo*)	−269.632 30					
5 (*exo*)	−269.630 16					
TS-**6**	−193.940 78	−193.986 06	−193.972 91		−193.987 81	0.103 92
TS-**7** (*endo*)			−592.782 98	−592.878 16	−592.880 61	0.121 09
TS–**8** (*exo*)			−592.780 44	−592.875 78	−592.878 45	0.120 86
TS-**9** (*endo*)			−270.188 70	−270.249 30	−270.251 84	
TS-**10** (*exo*)	−270.107 45		−270.187 00	−270.247 14	−270.249 77	
11	−345.635 33	−345.706 24				
12	−345.634 16	−345.704 92				
13	−345.635 32	−345.706 33				
14	−345.634 75	−345.705 53				
TS-**15**	−345.636 94	−345.707 86				0.143 54
TS-**16**	−345.635 03	−345.705 78				0.143 26
reactants						
OH radical		−75.536 15	−75.534 38	−75.547 57	−75.548 38	
H_2S			−398.810 10	−398.833 83		0.015 88
H_2O–O	−151.050 62	−151.071 56				0.026 89
H_2O		−76.207 33				

[a] The energies for TS-**7**, TS-**8**, and H_2S are frozen core. [b] Unless otherwise noted, the basis set for these energy calculations corresponds with the basis set used in the MP4/MP2 calculation on the structure. [c] Basis set is 6-31G* (full). [d] Basis set is 6-31G** (frozen core).

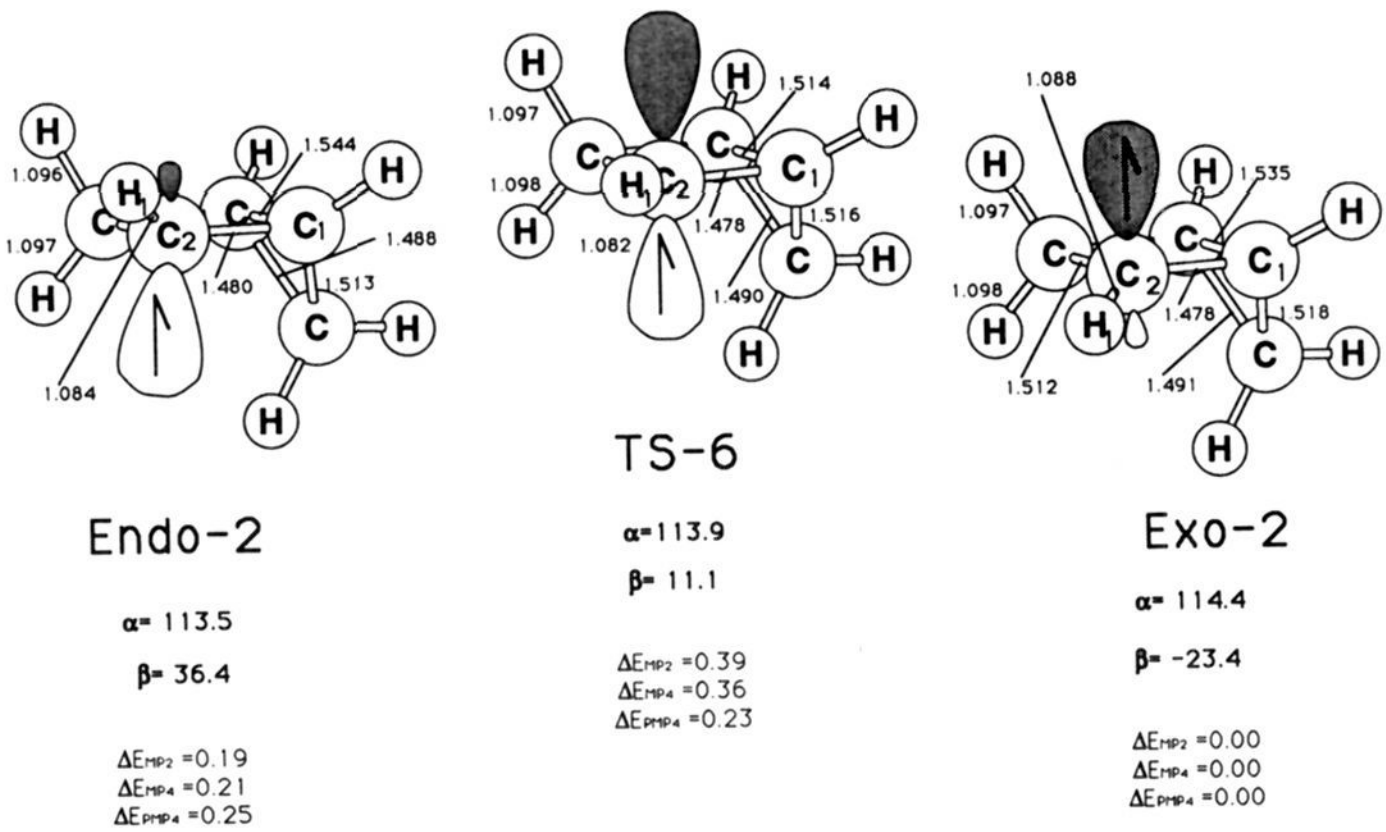

Figure 1. Geometries for *endo*- and *exo*-bicyclo[2.1.0]pent-2-yl radicals (**2**) and the transition state for inversion at the radical center (TS-**6**) at the MP2/6-31G* level showing the dihedral angle α between the plane of the two adjacent rings and dihedral angle β defining the deviation of the radical center from planarity. The relative energies are given in kilocalories/mole.

the MP2/3-21G and MP2/6-31G** levels. The increased steric interaction for *endo* trapping is reflected in the higher entropy of activation ($\Delta\Delta S^{\ddagger} = 1.1$ cal/mol K) for *endo* TS-**7**. The reported experimental $\Delta\Delta G^{\ddagger}$ was 1.1 kcal/mol.[7a] It is of interest to note that the *endo*-C-2 hydrogen bond is 0.027 Å longer than the *exo*–C–H bond in the transition state (Figure 2). The 10% S–H bond elongation in TS-**7** is also consistent with the relatively small isotope effect ($k_H/k_D = 1.85$) for reported[7a] *endo* trapping of **2**. The C_1–C_2 bond shortens and the C_1–C_5 bond elongates in the TS relative to hydrocarbon 1 (Figure 3) as a consequence of cyclopropylcarbinyl delocalization. Similar geometric changes are seen in the other transition states.

Hydrogen Abstraction by Hydroxyl Radical. Another of the fundamental questions that we wish to address in this study is the origin of the reactivity differences between the *endo*- and *exo*-C-2 hydrogens in bicyclo[2.1.0]pentane. At the MP2/6-31G** level the *endo*-C-2 hydrogen is 0.007 Å longer than the *exo*-C-2 hydrogen, reflecting a potentially weaker *endo*-C–H bond (Figure 3). However, *exo* and *endo* radicals **2** are of nearly identical energy, and the bond dissociation energies of the *exo*- and *endo*-C-2 hydrogen bonds must also be nearly identical. The greater reactivity of the *endo*-C-2 hydrogen must therefore be a consequence of a transition-state phenomenon.

The hydroxyl radical is one of the simplest open-shell oxygen species that we could use to model hydrogen abstraction from **1**. Hydrogen abstractions of this type require as a minimum the MP2 level of theory with a basis set that includes polarization functions on the hydrogen as well as the heavy atoms. The barrier height for abstraction of the *endo*-C-2 hydrogen from **1** by hydroxyl radical is predicted to be 6.81 kcal/mol at the MP4/6-31G**//MP2/6-31G** level of theory. Significantly, the *endo* activation barrier (TS–**9**) is 1.36 kcal/mol lower in energy than the transition state for abstraction of the *exo*-C-2 hydrogen (TS-**10**). The TS for hydrogen abstraction comes fairly early along the reaction coordinate since the C_2–H_2 bond in TS-**10** has only been elongated 0.08 Å relative to ground state **1**. However, the

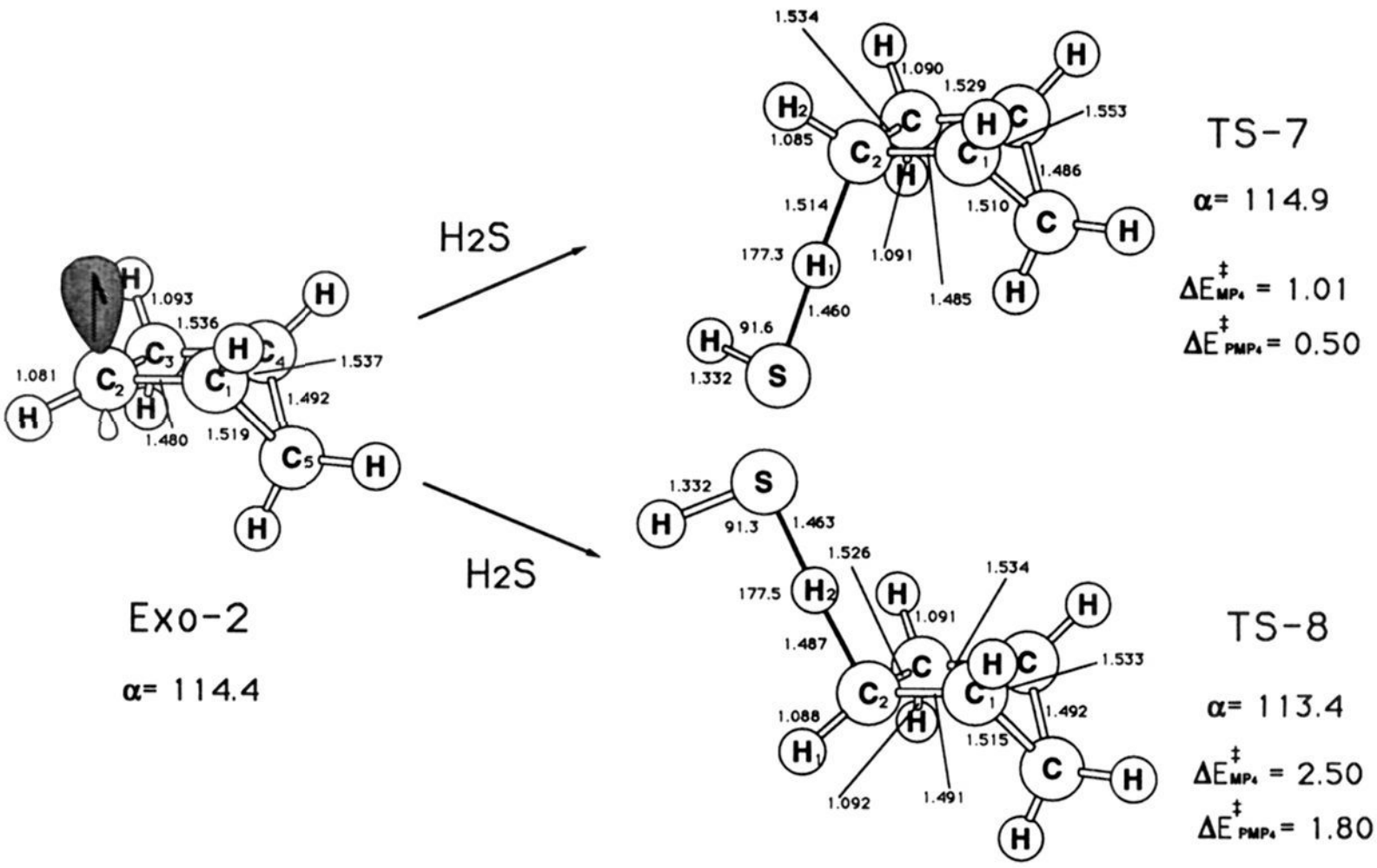

Figure 2. Transition structures for *endo* (TS-**7**) and *exo* (TS-**8**) trapping of the bicyclo[2.1.0]pent-2-yl radical (*exo*-**2**) by H_2S. Geometries at the MP2/6-31G** level show the dihedral angle α between the planes of the two adjacent rings. Activation energies at (P)MP4/6-31G**//MP2/6-31G** are given in kilocalories/mole.

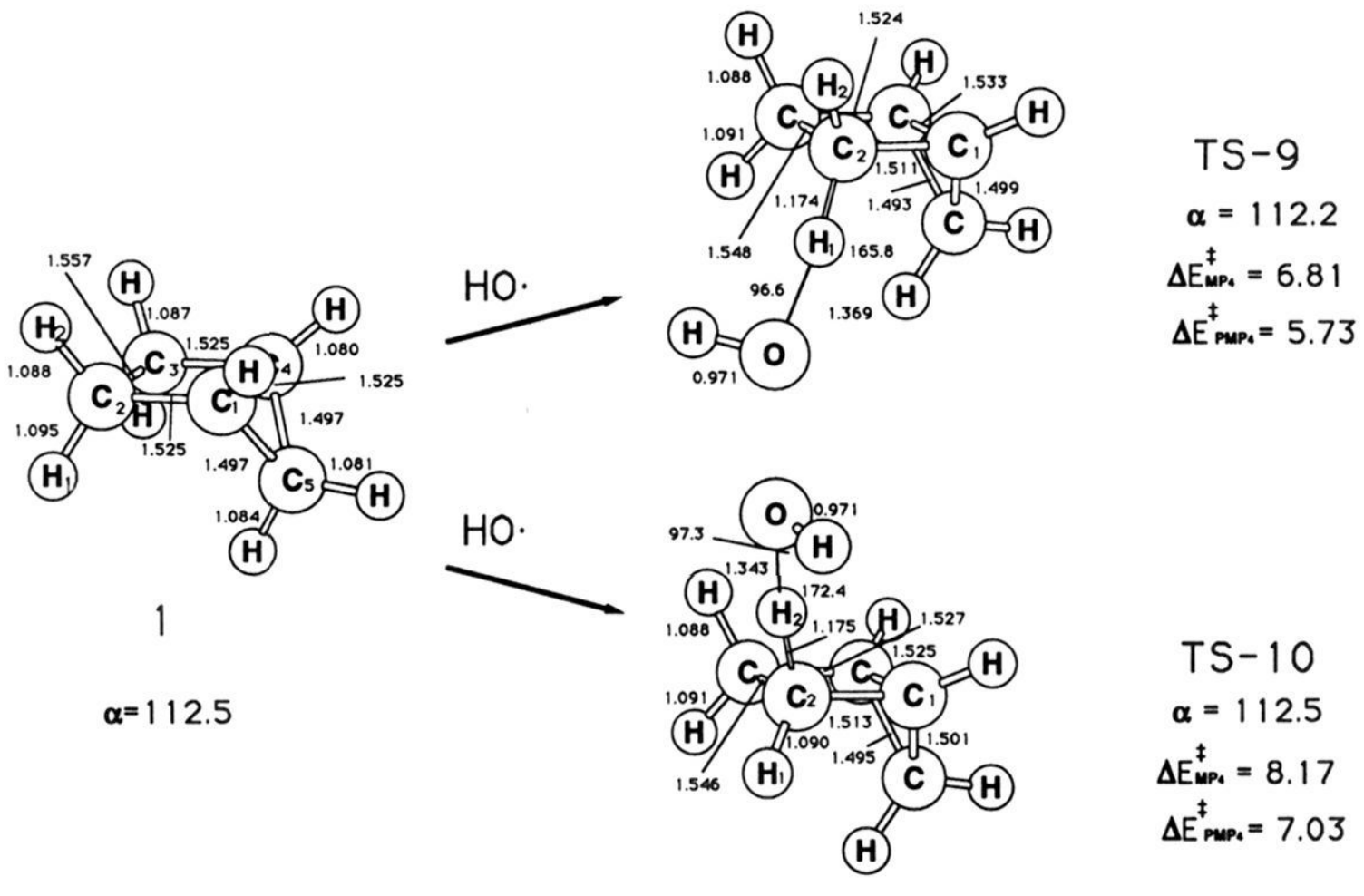

Figure 3. Transition structures for *endo* (TS-**9**) and *exo* (TS-**10**) hydrogen abstraction from bicyclo[2.1.0]pentane (**1**) by OH radical. Geometries optimized at the MP2/6-31G** level show the dihedral angle α between the planes of the two adjacent rings. Activation energies at (P)MP4/6-31G**//MP2/6-31G** are given in kilocalories/mole.

C_2–H_1 and C_2–H_2 bond lengths in TS-**9** and TS-**10** are essentially identical. The relatively low magnitude of this barrier height is also consistent with this exothermic (ΔE = –10.7 kcal/mol) hydrogen atom transfer reaction. The importance of removing unwanted spin states from the UHF wave function for hydrogen abstraction by HO has been established.[13] As expected, the PMP4/6-31G* barriers for TS-**9** and TS-**10** are lowered by 1.08 and 1.14 kcal/mol, respectively; nevertheless, the relative barriers (*endo* vs *exo*) consistently agree to within ±0.3 kcal/mol at the MP2, MP4, and PMP4 levels of theory. By comparison the barrier heights for the reaction $CH_4 + OH \rightarrow CH_3 + HOH$ with and without spin projection are 9.05 and 10.37 kcal/mol, respectively (MP4SDTQ/6-311G**).[13]

Since the difference in energy between *endo* and *exo* radical

(13) Gonzalez, C.; McDouall, J. J. W.; Schlegel, H. B. *J. Phys. Chem.* **1990**, *94*, 7467.

Scheme 2. Hydrocarbon Fragment Orbitals for a Disubstituted Methylene Group that Can Interact with an Electrophile E

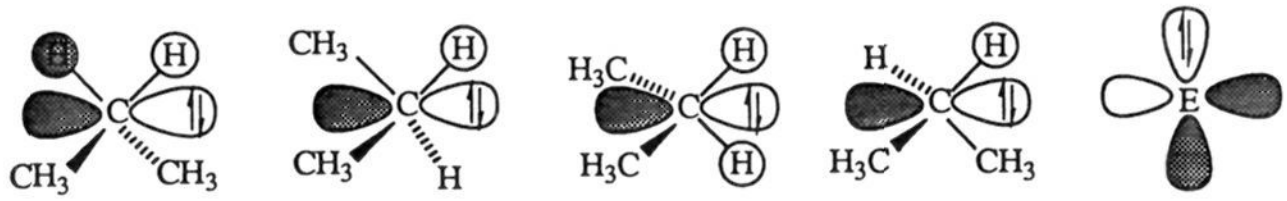

2 is extremely small, these data suggest that the faster rate of abstraction of the *endo*-C-2 hydrogen is attributable to a stabilizing stereoelectronic effect of the cyclopropylcarbinyl system in the transition state for abstracting the *endo* relative to the *exo*-C-2 hydrogen in **1**. Our calculations are consistent with the earlier work of Newcomb et al.[7] for the preferential trapping with ArSH on the *endo* face of radical **2**. Both experimental[7] and theoretical data implicate the adjacent cyclopropyl ring in **1** as the origin of the rate differences for both making and breaking the *endo*-C-2 hydrogen bond of **1**. Since the trapping of free radical **2** with Tempo does not involve C–H bond making, one should not anticipate a stereoelectronic influence, and the radical–radical recombination should be subject only to steric considerations. Both TS-**7** and TS-**9** may be considered as hydrogen abstraction (C_2–H) reactions from bicyclo[2.1.0]pentane by HS$^\bullet$ and HO$^\bullet$. Though one is a late TS and the other an early TS, both of the transition states are influenced stereoelectronically by the adjacent cyclopropyl ring.

Electrophilic Hydroxylation by Water Oxide. The above theoretical analysis and prior experimental data suggest that the stereoselectivity of *endo* hydroxylation is consistent with a stereoelectronic stabilization of the transition state affording secondary cyclopropylcarbinyl radical **2**. Although the weight of evidence for cytochrome P-450 hydroxylation supports the oxygen rebound mechanism, the possibility that a concerted oxene-insertion pathway intervenes with some enzymatic systems cannot be excluded. Ring opening of diphenyl-substituted cyclopropylcarbinyl radicals to give a rearranged radical has been measured to proceed at room temperature with exceptionally high rates ($k_r = 5 \times 10^{11}$ s^{-1}). In order for hydroxylation to proceed without rearrangement, k_{OH} must be greater than k_r (Scheme 1). Hydroxylation reactions have been observed where the oxygen rebound process would have to have occurred on the same time scale as a few molecular vibrations. Consequently, if this mechanism is actually involved, the rate of reaction between a carbon radical center and iron-bound hydroxyl radical can occur with sufficient velocity to give the appearance of a concerted process.[6] Iron-mediated hydroxylation of 2,2-diphenylmethylcyclopropane by methane monooxygenase (MMO) gave no rearranged alcohol despite the fact that k_r for this radical is 5×10^{11} s^{-1}.[14] A two-step radical rebound process would require that k_{OH} be greater than 4×10^{13} s^{-1}.[14] These data lend credence to the suggestion that carbon–oxygen bond formation may not proceed through formation of a cyclopropylcarbinyl radical or cation. Hydroxylation of bicyclo[2.1.0]pentane with cytochrome P-450 afforded only *endo* alcohol **4** (Scheme 1),[1] while MMO gave approximately an equal amount of *exo* and *endo* insertion products.[14] Cogent arguments were presented that MMO hydroxylation with selected substrates can involve direct oxygen insertion without the intermediacy of a free radical. This interesting mechanistic dichotomy promoted us to examine the *endo*/*exo* stereoselectivity for electrophilic hydroxylation of bicyclo[2.1.0]pentane.

We have recently described a frontier molecular orbital (FMO) model for the activation of saturated hydrocarbons that provides a rationale for the orientation of approach of the electrophile and an explanation for the observed stereoselectivity for insertions into carbon–hydrogen bonds.[15a,b] In this FMO model we dissect the hydrocarbon into doubly occupied fragment orbitals that have σ- and π-symmetry. For example, pertinent canonical Hartree–Fock molecular orbitals for the secondary carbon of propane are given in Scheme 2. In this model the electrophile E has an empty electrophilic orbital and one or more pairs of electrons that serve as the terminus for a concerted 1,2-hydrogen migration in the transition state for electrophilic insertion of E into a C–H bond. In the transition state the electrophile E approaches the fragment orbital along the axis of the filled atomic carbon p orbital, and a 1,2-hydrogen migration to an adjacent lone pair of electrons takes place in concert with C–E bond formation. The localized description of the C–H bond is equally valid, but it is more difficult to visualize the trajectory of the electron-donating and accepting orbitals.

Water oxide has recently been predicted to exist as an energy minimum on the potential energy surface for the 1,2-hydrogen

Scheme 3

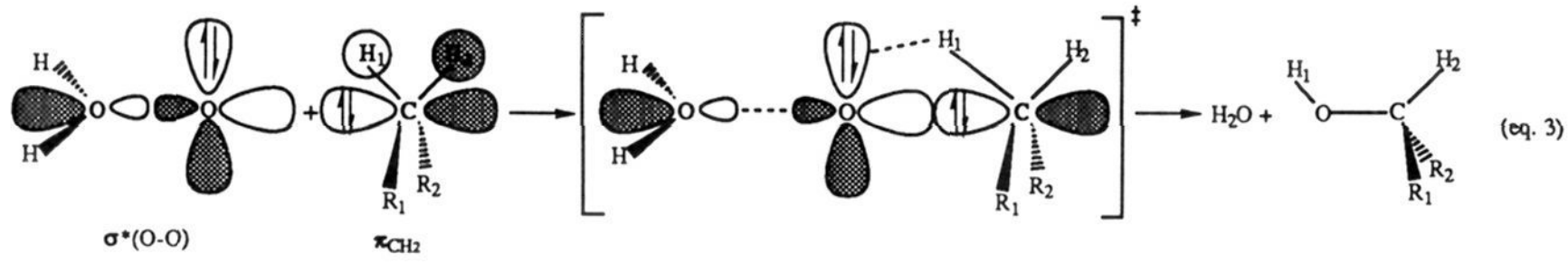

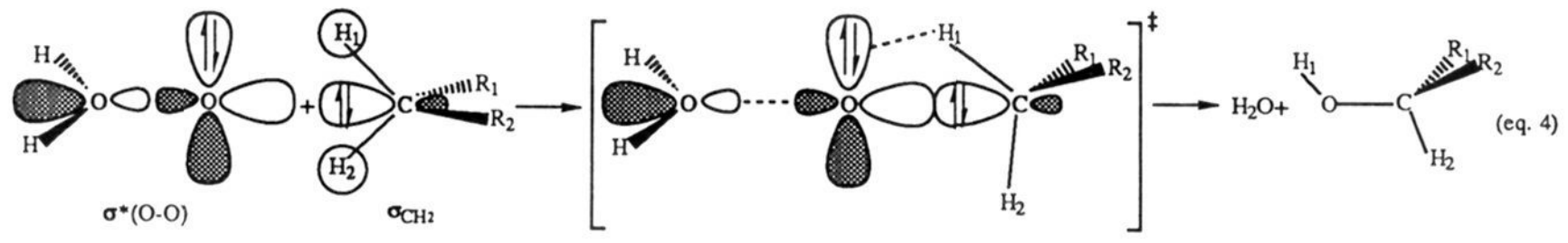

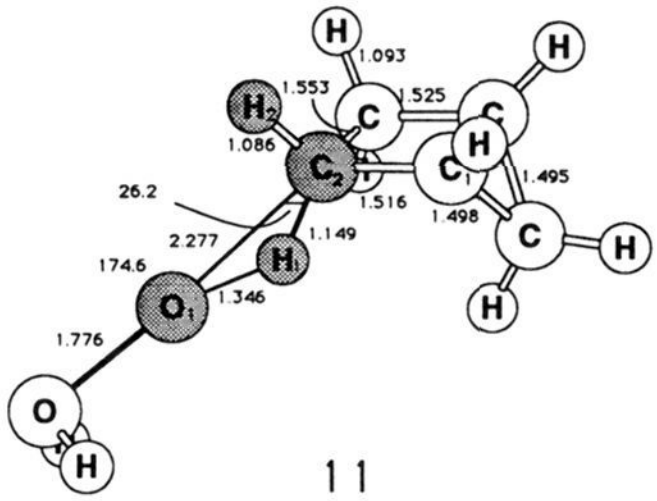

11

σ CH2 Orientation

$\Delta E^{\ddagger}_{MP2}$ = 8.95

$\Delta E^{\ddagger}_{MP4}$ = 6.34

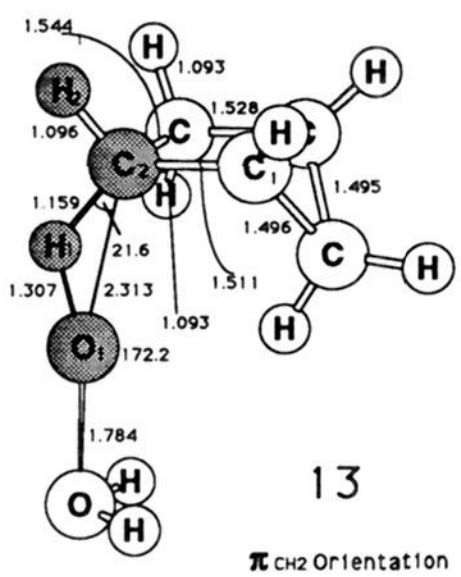

13

π CH2 Orientation

$\Delta E^{\ddagger}_{MP2}$ = 8.95

$\Delta E^{\ddagger}_{MP4}$ = 6.29

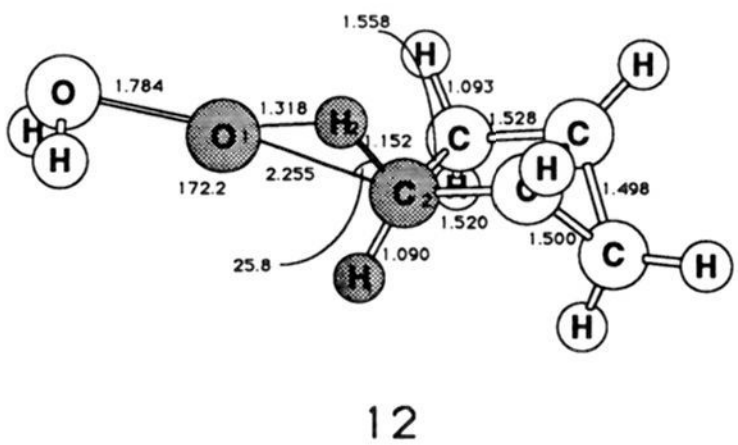

12

σ CH2 Orientation

$\Delta E^{\ddagger}_{MP2}$ = 9.68

$\Delta E^{\ddagger}_{MP4}$ = 7.17

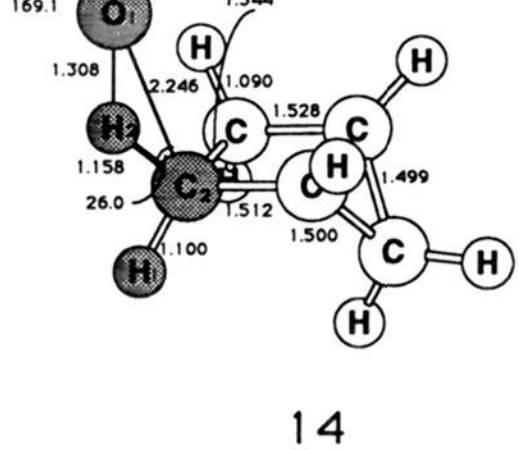

14

π CH2 Orientation

$\Delta E^{\ddagger}_{MP2}$ = 9.31

$\Delta E^{\ddagger}_{MP4}$ = 6.79

Figure 4. Idealized *endo* σCH_2 (**11**), *exo* σCH_2 (**12**), *endo* πCH_2 (**13**), and *exo* πCH_2 (**14**) orientations for oxygen atom transfer from water oxide to bicyclo[2.1.0]pentane. Structures **11** and **12** are SOSP, while **13** and **14** have nonzero gradients. The dihedral angle of the shaded atoms in each figure is constrained to be planar. Geometries are at the MP2/6-31G* level, distances are given in angstroms, and angles are in degrees. Barrier heights are given in kilocalories/mole.

migration in hydrogen peroxide (HOOH → H_2OO).[15c,16] We have utilized water oxide (H_2O–O) as a model oxygen atom donor in the oxidation of amines to amine oxides[15c] and the oxidation of saturated hydrocarbons to alcohols.[15a] We have established that the MP2/6-31G* level of theory is adequate for predicing geometries and fourth-order Møller–Plesset perturbation theory (MP4) for describing potential energy surfaces involving heterolytic cleavage of the O–O bond in water oxide.[15d]

In earlier studies on a series of saturated hydrocarbons we found that electrophilic oxygen approaches the hydrocarbon along the atomic p orbital comprising a π_{CH_2} fragment orbital (Scheme 2),[15a] while carbene insertion typically involves interaction with a doubly occupied σ_{CH_2} fragment orbital.[15b] Interaction of both electrophiles with π_{CHCH_3} and σ_{CHCH_3} orbitals gave higher activation barriers due to increased steric interactions. The primary pathway for oxygen atom insertion in the π_{CH_2} orientation can be envisaged as the interaction of the empty σ^* orbital of the O–O bond of water oxide with the doubly occupied π_{CH_2} fragment orbital. In the transition state the CH_1 bond is broken as hydrogen H_1 migrates the adjacent oxygen, affording the alcohol insertion product (eq 3). In a similar fashion the σ_{CH_2} orbital can mix with the σ^*_{O-O} orbital and displace water as a neutral leaving group in concert with hydrogen migration (eq 4) (see Scheme 3).

Because of the structural complexity of the bicyclic hydrocarbon **1** and the number of basis functions involved (135), we first examined "idealized transition states" for *endo* and *exo* oxygen insertion by water oxide (Figure 4). In these orientations the O_1–C_2–H_1–H_2 dihedral angle is constrained to be planar. Molecular models suggest that the least sterically hindered pathways for oxygen atom transfer to **1** would appear to be σ_{CH_2} *endo* and *exo* orientations **11** and **12** (Figure 4). The *endo* insertion pathway **11** is 0.83 kcal/mol lower in energy than corresponding *exo* insertion **12**, involving migration of hydrogen H_2 at the MP4//MP2/6-31G* level (Table 1). However,

(14) Liu, K. E.; Johnson, C. C.; Newcomb, M.; Lippard, S. J. *J. Am. Chem. Soc.* **1993**, *115*, 939.

(15) (a) Bach, R. D.; Andrés, J. L.; Su, M.-D.; McDouall, J. J. W. *J. Am. Chem. Soc.* **1993**, *115*, 5768. (b) Bach, R. D.; Su, M.-D.; Aldabbagh, E.; Andrés, J. L.; Schlegel, H. B. *J. Am. Chem. Soc.* **1993**, *115*, 10237. (c) Bach, R. D.; Owensby, A.; Gonzalez, C.; Schlegel, H. B.; McDouall, J. J. W. *J. Am. Chem. Soc.* **1991**, *113*, 6001. (d) Bach, R. D.; Andrés, J. L.; Owensby, A.; Schlegel, H. B.; McDouall, J. J. W. *J. Am. Chem. Soc.* **1992**, *114*, 7207.

(16) Meredith, C.; Hamilton, T. P.; Schaeffer, H. F., III. *J. Phys. Chem.* **1992**, *96*, 9250.

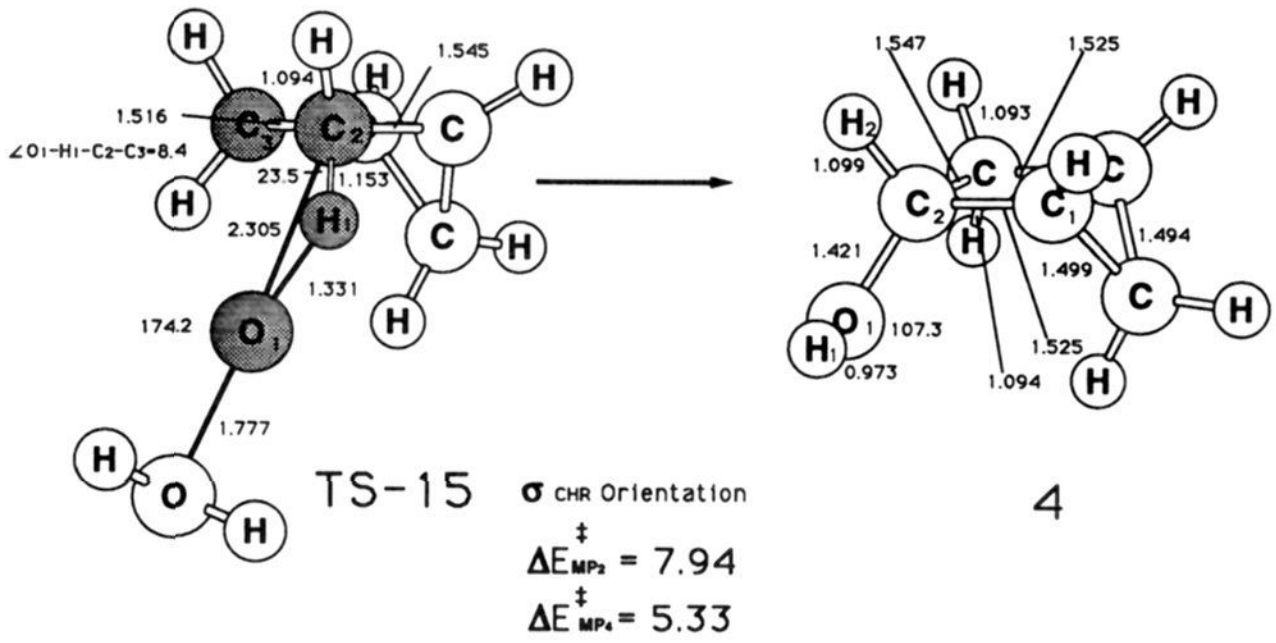

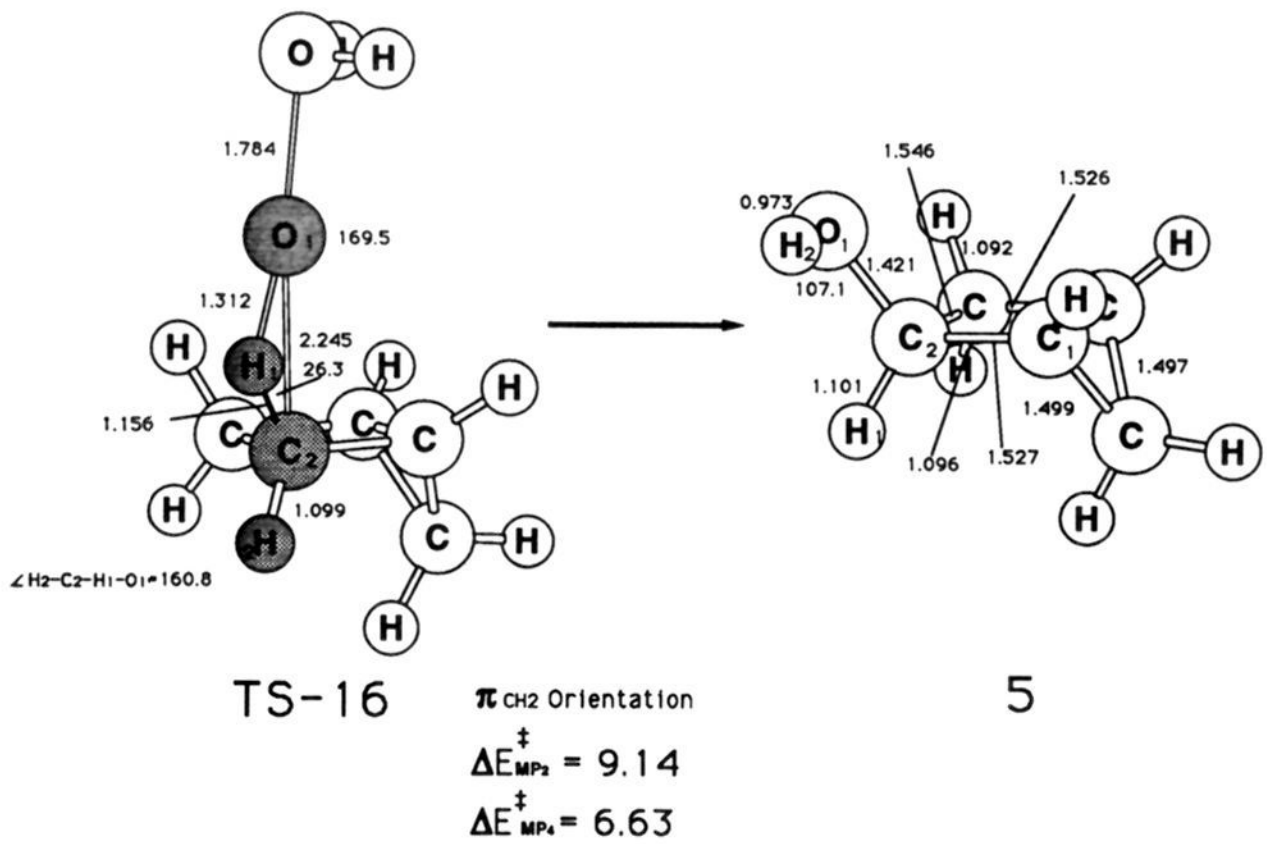

Figure 5. Fully optimized transition states for oxygen insertion into C–H bonds of bicyclo[2.1.0]pentane (**1**) with the approximate *endo* σCHR (TS-**15**) and *exo* πCH_2 (TS-**16**) orientations and the *endo* (**4**) and *exo* (**5**) alcohol products of hydroxylation. Geometries are at the MP2/6-31G* level, distances are given in angstroms, and angles are in degrees. Activation energies at MP4/6-31G*//MP2/6-31G* and MP2/6-31g* are given in kilocalories/mole.

analytical frequency calculations established both structures to be second-order saddle points (SOSP). The second imaginary frequency corresponds to a rotation from the σ_{CH_2} to the *endo* σ_{CHR} orientation (see TS-15).

The geometrically constrained π_{CH_2} orientations for *endo* (**13**) and *exo* (**14**) hydroxylation were also examined, and all variables were optimized with the exception of the O_1–C_2–H_1–H_2 dihedral angle denoted by the shaded atoms (Figure 4). The two pathways differed by only 0.50 kcal/mol, with a slight preference being observed for insertion into the *endo* C_2–H_1 σ bond (Table 1). However, both "transition structures" had nonzero forces in the constrained dihedral angle. Release of this geometry constraint resulted in fully optimized transition structures (Figure 5) that were confirmed to be first-order saddle points by analytical frequency calculations at the MP2/6-31G* level. The barrier for the *endo* approach in TS-15 was 1.3 kcal/mol lower in energy than *exo* TS-16. The ZPE corrections for TS-15 and TS-16 are −1.97 and −2.15 kcal/mol, respectively. This fully optimized *exo* transition structure is only 0.16 kcal/mol lower in energy than the idealized π_{CH_2} approach in **14** (Figure 4). The H2–C2–H1–O1 dihedral angle in TS-**16** deviates 19.2° from planarity. The overall reaction trajectory is approximately π_{CH_2} in nature. The lowest energy pathway for oxygen atom insertion (TS-**15**) corresponds to the more sterically hindered approach. The orientation of oxygen attack from the *endo* direction involves interaction of the occupied H_1–C_2–C_3 hydrocarbon fragment orbital (π_{CHR}) shown in Scheme 2 with the empty σ^*_{O-O} orbital of water oxide. The O_1–H_1–C_2–C_3 dihedral angle in TS-**15** is only 8.4° out-of-plane. Electronic factors appear to favor the more hindered σ_{CHR} approach. The barrier height for TS-**15** (5.33 kcal/mol) is 1.0 kcal/mol lower in energy than the idealized *endo* σ_{CH_2} approach described in SOSP 11 (Figure 4). By comparison, the activation energy for the comparable oxidation of propane at C_2 is 3.9 kcal/mol for the π_{CH_2} orientation.[15a] We suggest that the cyclopropylcarbinyl stabilization of the developing positive charge attending hydrocarbon migration is largely responsible for the *endo* selectivity observed. The alcohol insertion products **4** and **5** were fully optimized at the MP2/6-31G* level, and *endo* alcohol **4** is predicted to be more stable than its *exo* isomer by 1.3 kcal/mol.

We conclude from these data that the cyclopropylcarbinyl moiety in bicyclo[2.1.0]pentane (**1**) can exert its stereoelectronic influence on both the free-radical and electrophilic pathways for hydroxylation. This raises a question about the differences in the active site for P-450 versus MMO hydroxylation of **1**. Since it appears that electronic effects slightly favor *endo* hydroxylation, the lack of *endo*/*exo* selectivity in MMO hydroxylation could be attributed to less steric requirements at the active site.[14] However, this suggestion must be reconciled with a rebound rate (k_{OH}) that is greater than the rate of radical rearrangement ($k_r = 1.5 \times 10^9$

s^{-1}).[6,7] If hydrogen abstraction occurs from the *endo* face of **1**, then in order to form the *exo* alcohol in accordance with Scheme 1, either substrate **1** must rotate to expose its *exo* face or the hydroxyl radical must migrate to the *exo* face of radical **2**. Reduced mass considerations militate against dynamic motion of either the iron center or the higher molecular weight hydrocarbon substrates on the reaction surface for the oxygen rebound step (k_{OH}). Dynamic rate theory considerations suggest that the lighter hydroxyl radical should migrate to the carbon radical center in the bound substrate in the rebound step. The frequency factor $k_T/h \sim 10^{13}$ seems to be the upper limit for rates of chemical change where nuclei, rather than just electrons or energy, change their position. The hydroxyferryl complex and the carbon–radical center must constitute an "intimate complex" in order for the Fe–OH bond to homolytically break and form a C–OH bond with rate constants approaching 10.[13] Consistent with this concept, an increase in molecular size of the hydrocarbon substrate could result in a greater van der Waals attraction for the charged ferryl center, a tighter binding, and a faster rebound rate as a consequence of its increasing polarizability. As the polarizability of the neutral becomes larger, a charge-induced dipole force can result in a deepening of the initial electrostatic potential well, and in principle this could overcome the intrinsic barrier to hydroxyl insertion. In the case of methane hydroxylation by MMO both carbon and oxygen radicals are of approximately equal mass and both could migrate accordingly in the rebound step. The above arguments are consistent with a concerted oxygen insertion process for those hydrocarbon substrates that exhibit very rapid radical rearrangement (k_r).[7c]

Acknowledgment. This work was supported in part by the National Science Foundation (CHE 90-20398), a NATO Collaborative Research Grant (900707), and the Spanish "Ministerio de Educacion". We are also thankful to the Pittsburgh Supercomputing Center, CRAY Research, and the Ford Motor Co. for generous amounts of computer time.